

Interpreting large-scale redshift-space distortion measurements

L. Samushia,^{1,2*} W. J. Percival,¹ and A. Raccañelli¹

¹ *Institute of Cosmology and Gravitation, University of Portsmouth, Dennis Sciana Building, Portsmouth PO1 3FX, U.K.*

² *National Abastumani Astrophysical Observatory, Ilia State University, 2A Kazbegi Ave., GE-1060 Tbilisi, Georgia*

8 March 2017

ABSTRACT

The simplest theory describing large-scale redshift-space distortions (RSD), based on linear theory and distant galaxies, depends on the growth of cosmological structure, suggesting that strong tests of General Relativity can be constructed from galaxy surveys. As data sets become larger and the expected constraints more precise, the extent to which the RSD follow the simple theory needs to be assessed in order that we do not introduce systematic errors into the tests by introducing inaccurate simplifying assumptions. We study the impact of the sample geometry, non-linear processes, and biases induced by our lack of understanding of the radial galaxy distribution on RSD measurements. Using LasDamas simulations of the Sloan Digital Sky Survey II (SDSS-II) Luminous Red Galaxy (LRG) data, these effects are shown to be important at the level of 20 per cent. Including them, we can accurately model the recovered clustering in these mock catalogues on scales 30–200 h^{-1} Mpc. Applying this analysis to robustly measure parameters describing the growth history of the Universe from the SDSS-II data, gives $f(z = 0.25)\sigma_8(z = 0.25) = 0.3930 \pm 0.0457$ and $f(z = 0.37)\sigma_8(z = 0.37) = 0.4328 \pm 0.0370$ when no prior is imposed on the growth-rate, and the background geometry is assumed to follow a Λ CDM model with the WMAP + SNIa priors. The standard WMAP constrained Λ CDM model with General Relativity predicts $f(z = 0.25)\sigma_8(z = 0.25) = 0.4260 \pm 0.0141$ and $f(z = 0.37)\sigma_8(z = 0.37) = 0.4367 \pm 0.0136$, which is fully consistent with these measurements.

Key words: cosmological parameters — dark energy — large-scale structure of Universe

1 INTRODUCTION

The statistical quantification of Redshift-Space Distortions (RSD) provides a robust method for measuring the growth of structure on very large scales. RSD arise because we infer galaxy distances from their redshifts using the Hubble law: the radial component of the peculiar velocity of individual galaxies will contribute to the redshift and therefore alter our estimate of the distances to them. The measured clustering of galaxies will therefore be anisotropic and the additional radial signal can be used to determine the characteristic amplitude of the pair-wise distribution of the peculiar velocities at a given scale, which in turn depends on the growth rate.

Many previous analyses have used RSD to measure the cosmological growth rate using both the correlation function and power spectrum (see, for example, Hawkins et al. 2003;

Percival et al. 2004; Zehavi et al. 2005; Tegmark et al. 2006; Guzzo et al. 2008; Cabré & Gaztañaga 2009; Song et al. 2010). In general these studies used clustering information over a small range of scales, and a simplified modelling procedure in order to make the measurements.

Large-scale RSD measurements provide results that can be compared to direct measurements of peculiar velocities in the local Universe: both observations depend on the amplitude of the velocity field. Recent analyses of the local data seem to indicate the presence of unexpectedly large bulk flows, 2σ higher than Λ CDM predictions (Watkins et al. 2009; Feldman et al. 2010; Macaulay et al. 2011), although Nusser & Davis (2010) present more compatible measurements. Large bulk velocities were also detected through measurements of the kinetic Sunyaev-Zeldovich effect on the X-ray cluster catalog (Kashlinsky et al. 2009). The excess velocities detected are at odds with the previous RSD measurements from the 2-degree Field Galaxy Redshift Survey (2dFGRS; Colless et al. 2003) and the Sloan Digital Sky Survey

* email: lado.samushia@port.ac.uk

(SDSS; York et al. 2000) discussed above, which give results broadly consistent with Λ CDM models. There is therefore strong motivation for considering if systematic effects could be affecting either set of observations.

If we assume that observed galaxies are sufficiently far away that their separations are small compared to the distances between them and the observer (the “plane-parallel” approximation) then, to linear order, the relationship between the redshift-space galaxy power-spectrum P_{gg}^{s} , the real-space matter power-spectrum P_{mm}^{r} and the growth rate is simple (Kaiser 1987; Hamilton 1997),

$$P_{\text{gg}}^{\text{s}}(k, \mu) = P_{\text{mm}}^{\text{r}}(k)(b + f\mu^2)^2, \quad (1)$$

where b accounts for a linear deterministic bias between galaxy and matter overdensity fields, f is the logarithmic derivative of the growth factor by the scale factor $f \equiv d \ln G / d \ln a$, and μ is the cosine of the angle to the line-of-sight. In our paper we study possible theoretical systematics beyond the model of Eq. (1), that could effect the measurements of clustering on large scales including the effects due to wide-angle corrections, large-scale nonlinearities, sample geometry and the effects of the radial model for the distribution of galaxies.

Nonlinear effects change the real-space matter power spectrum, the velocity power spectrum, the matter–velocity cross-correlation, and introduce further μ dependent terms into this expression (Scoccimarro 2004). On small scales the dominant nonlinear contribution comes from the Fingers-of-God (FOG) effect (Jackson 1972). FOG arise because within dark matter halos the velocities of galaxies quickly become virialized and their power-spectrum is highly nonlinear. This effect can be approximated by including a phenomenological term in Eq. (1) that reduces power on small scales (Peacock & Dodds 1996) or using a more complicated expression based on higher order computations in perturbation theory (see e.g., Scoccimarro 2004; Taruya 2010). The phenomenological damping terms used to describe the FOG effects are not accurate (Scoccimarro 2004; Jennings et al. 2011) and the results of perturbation theory are not easy to implement in a computationally fast and efficient way. The effects of nonlinear growth on the real-space power-spectrum are also important and difficult to model for an arbitrary cosmological model. Although in principle these nonlinear effects can be estimated analytically using perturbation theory, comparison of different perturbation theory methods to the results of high-resolution N-body simulations shows that at low redshifts the range of scales where the perturbation theory is reliable is rather small (Carlson et al. 2009). In addition, the assumption that the bias between matter overdensities and galaxies is linear is not accurate even for the scales as large as $30 h^{-1}$ Mpc (Okamura & Jing 2011).

Wide-angle corrections are needed because, if the angle α that a galaxy pair forms with respect to the observer is large, the distance between galaxies is comparable to their distance to the observer and the “plane-parallel” approximation (and hence Eq. 1) breaks down. The redshift-space correlation function and the power-spectrum in this case will also depend on the third variable that could be chosen to be the angle α . The wide-angle linear redshift-space correlation function and power-spectrum as a function of all three variables have been computed (Zaroubi & Hoffman 1993; Szalay et al. 1998; Szapudi 2004; Matsubara 2004;

Papai & Szapudi 2008). In fact, the wide-angle correlation function does not deviate significantly from its “plane-parallel” counterpart if the opening angle is less than 10° . In previous work we validated this work by analysing mock galaxy catalogs (Raccanelli et al. 2010).

For surveys that cover a significant fraction of the sky, the distribution of galaxies pairs becomes non-trivial. The survey geometry results in the galaxy pair distribution that has a complicated dependence on the variables r , μ and α , since not all sets of their combinations are equally likely or even geometrically possible. In particular the distribution of μ does not correspond to that of an isotropic pair distribution. This will strongly bias the measurement of angular momenta of the correlation function, and in fact, often dominates over differences between “plane-parallel” and “wide-angle” effects for typical galaxy pairs (Raccanelli et al. 2010).

RSD data on very large scales, although in principle available in current data sets, do not contribute significantly to current data analyses. The reason for this is twofold: the signal-to-noise of currently available clustering data becomes low at scales larger than $100 h^{-1}$ Mpc so most of the available cosmological information is on smaller scales; also the large scale clustering measurements are vulnerable to different observational (improper modelling of seeing, galactic extinction, etc.) and theoretical systematic effects which, if not taken into account properly, could strongly bias results of data analysis. In particular, our ability to model the radial galaxy distribution accurately can cause strong effects on these large-scales, and is worthy of further investigation (Percival et al. 2010; Kazin et al. 2010). Being able to model these data has many advantages. First, if accurate measurements are available, more data will result in stronger constraints on cosmological parameters. In addition, measurements on large scales are significantly less affected by the systematics introduced by nonlinear phenomena. Some important physical processes can be measured only on very large scales. For example, non-Gaussian initial conditions, if present, will effect the real-space galaxy clustering on large scales (Dalal et al. 2008; Desjaques & Seljak 2010), and could be compared against the RSD signal, which depends on the matter field.

We investigate the significance of these effects by performing an analysis on large suite of N-body simulations, testing for systematic effects that could result in real data giving a signal different from the plane-parallel linear RSD formula. Using mock samples, we are able to accurately fit the expected correlation function on scales between 30 – $200 h^{-1}$ Mpc, to a level well below the statistical error on the measurement from any one sample.

We apply the knowledge learned in this analysis to robustly measure RSD in the Sloan Digital Sky Survey (SDSS) Data Release 7 (DR7) sample of Luminous Red Galaxies (LRGs) and measure cosmological parameters describing amplitude and growth of the perturbations in different models. We find that the accuracy of SDSS DR7 data is at the threshold where the inclusion of RSD information on very large scales affects the measurements but does not improve the result significantly. In contrast, the non-linear and survey geometry effects are significant. The next generation of spectroscopic surveys, such as *BOSS* (Schlegel et al. 2009), *BigBOSS* (Schlegel et al. 2009) and *EUCLID* (Laureijs et al.

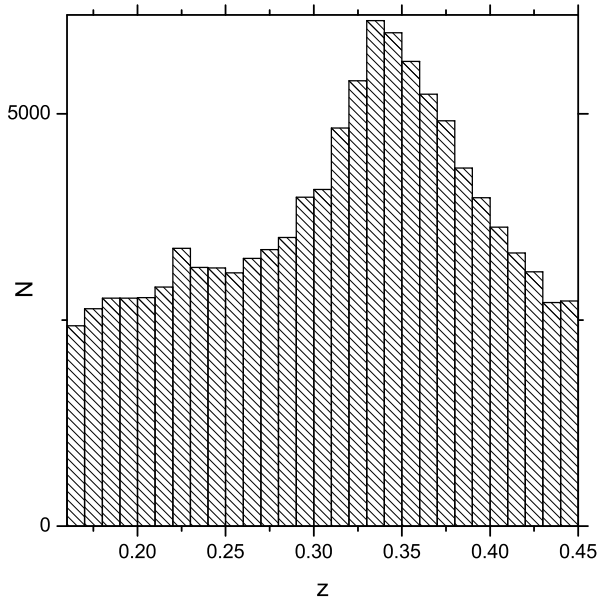


Figure 1. Histogram showing the redshift distribution of galaxies in the SDSS DR7 LRG catalog used in our analysis.

2009) will enable us to measure the clustering of galaxies at large scales with extremely high accuracy and using RSD data on large scales will be crucial for constraining growth of structure in the Universe and the nature of gravity in a robust way. For these future high precision measurements, the systematic effects on very large scales may well be significantly easier to model compared to small scales systematics due to different nonlinear factors.

This paper is organised as follows, in Sec. 2 we describe our data set and the method of measurement. In Sec. 3 we present our theoretical model for the RSD on very large scales and check its validity with the results of N-body simulations. In Sec. 4 we describe theoretical models and assumptions made when extracting cosmologically relevant information. In Sec. 5 we present results of our data analysis. In Sec. 6 we conclude and discuss the relevance of the contents of our paper to future spectroscopic galaxy surveys.

2 CALCULATING MOMENTA OF THE CORRELATION FUNCTION

2.1 The SDSS data

We use data from the SDSS, which obtained wide-field CCD photometry (Gunn et al. 1998) in five passbands (u, g, r, i, z ; e.g., Fukugita et al. 1996), amassing nearly 10,000 square degrees of imaging data for which object detection is reliable to $r \sim 22$ (Abazajian et al. 2009). From these photometric data, luminous red galaxies were targeted (Eisenstein et al. 2001) and spectroscopically observed, yielding a sample of 106,341 LRGs in the redshift bin $0.16 < z < 0.44$. The redshift distribution of galaxies in this catalog is shown on Fig. 1.

To study clustering properties of LRGs we create a random catalog that has unclustered “galaxies” randomly distributed with the same angular mask as SDSS DR7. The angular distribution of these galaxies was chosen as described

in Reid et al. (2009). The method for, and effect of estimating the expected radial distribution of the galaxies is described in Section 2.3. Our random catalog has approximately 50 times more objects than the real catalog.

2.2 Methodology

We assign each galaxy a weight

$$w = \frac{1}{1 + n(\mathbf{r})\bar{P}}, \quad (2)$$

where $n(\mathbf{r})$ is a local density of galaxies in units of $(h^{-1} \text{ Mpc})^{-3}$ in a neighbourhood of the galaxy of interest located at a position \mathbf{r} and $\bar{P} = 10000 (h^{-1} \text{ Mpc})^3$. This weighting is optimal for the premise that galaxies Poisson sample the underlying matter field (Feldman et al. 1994). Recent work has shown that it may be possible to beat this if we can estimate the mass associated with each galaxy (Seljak et al. 2009): we do not attempt this in this work.

In order to extract information about the evolution of structure growth, we divide the LRG sample in two redshift bins so that the weighted number of galaxies

$$N_w = \sum_i w_i, \quad (3)$$

is approximately equally split between them. The effective redshifts for our two bins are $z = 0.25$ and $z = 0.37$.

For each pair of objects in our galaxy catalog, random catalog or cross pairs between galaxy and random catalogs, we compute the distance between objects r , the angle α that the objects make with respect to us, and the cosine of the angle that the bisector of the angle between the objects makes with the line connecting them (assuming a flat geometrical model) μ . Due to statistical isotropy about the observer, these three variables are sufficient to completely describe the RSD expected for each pair. We bin r in 65 equal logarithmic bins from $1 h^{-1} \text{ Mpc}$ to $200 h^{-1} \text{ Mpc}$, μ in 200 equal bins from 0 to 1, $\cos(\alpha)$ in 400 bins from 0 to 1 and count the number of galaxies in each bin.

To convert angular and redshift separations of galaxies into physical separations a fiducial cosmological model is needed. We compute distances in a spatially-flat ΛCDM fiducial model. If the real geometry of the Universe is different from the one described by our fiducial model it will bias the measurements of clustering through the Alcock-Paczynski effect. We discuss this issue in Sec. 3.5.

In the plane-parallel approximation, all of the available linear RSD information can be extracted from the zeroth, second and fourth Legendre momenta of the galaxy correlation function with respect to the variable μ (Hamilton 1992). Given that we expect that wide-angle and non-linear effects will give relatively small deviations about this approximation, we should expect that, even in the more general case, these momenta contain almost all of the available RSD information. We therefore choose to fit to these measurements in our work. This will be discussed further in Section 3. To estimate those three we use Landy-Szalay type estimators (Landy & Szalay 1993)

$$\hat{\xi}_\ell(r_i) = \sum_{j,k} [DD(r_i, \mu_j, \alpha_k) - 2DR(r_i, \mu_j, \alpha_k)]$$

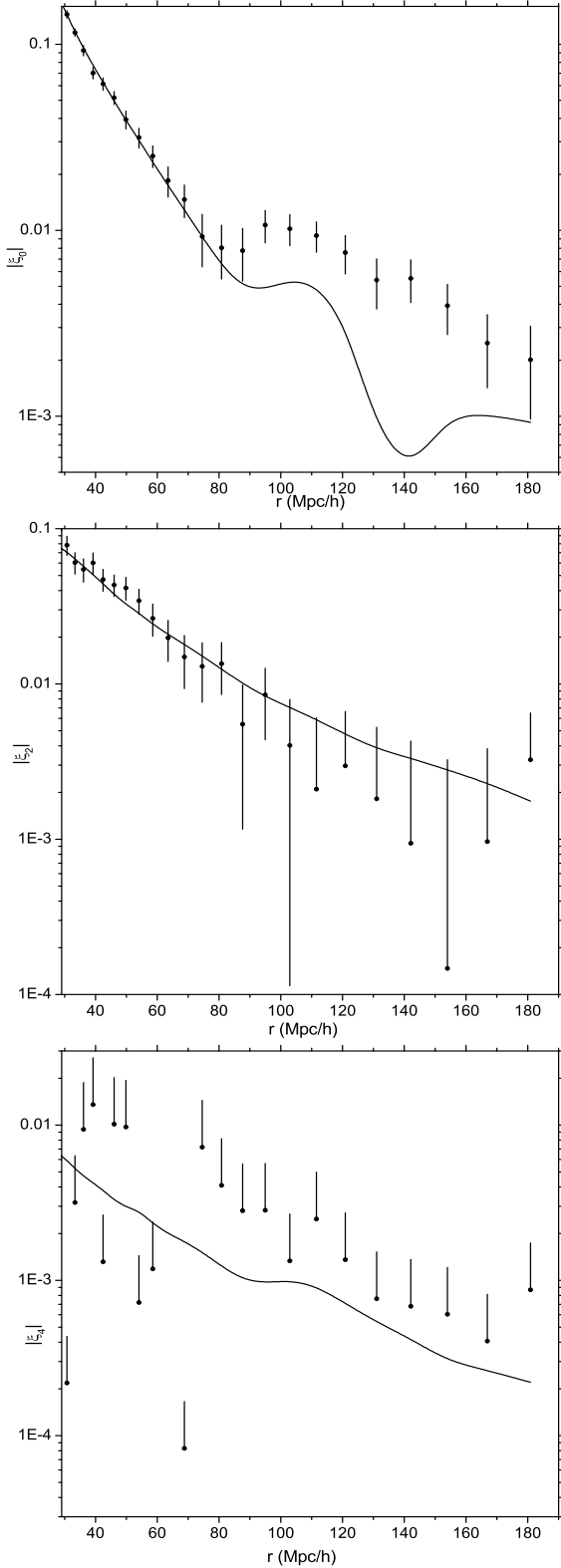


Figure 2. Measurements of $\hat{\xi}_\ell(r)$ from SDSS DR7 LRG in a redshift range $0.16 < z < 0.44$. The statistical error-bars were calculated as described in Section 3 and represent only the diagonal elements of the whole covariance matrix. The absence of lower error-bar on some measurements indicates that they are consistent with zero.

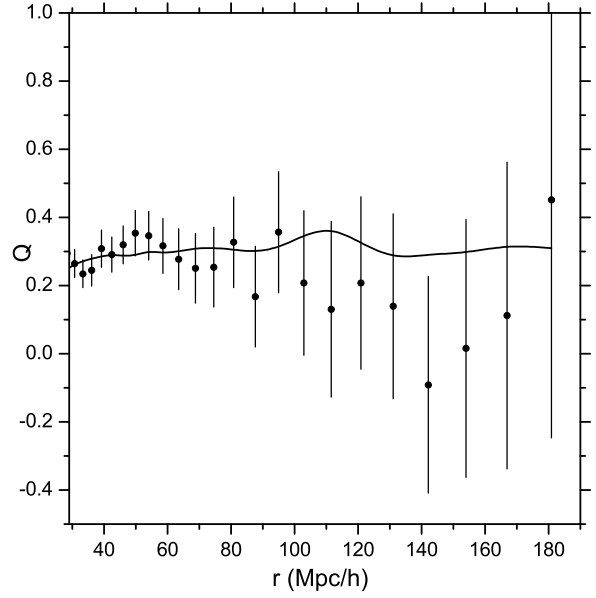


Figure 3. Measurements of $\hat{Q}(r)$ from SDSS DR7 LRG in a redshift range $0.16 < z < 0.44$. Error-bars were calculated as described in Section 3 and show only the diagonal elements of statistical covariance matrix.

$$+RR(r_i, \mu_j, \alpha_k)] P_\ell(\mu)/RR(r_i, \mu_j, \alpha_k), \quad (4)$$

where $DD(r_i, \mu_j, \alpha_k)$, $DR(r_i, \mu_j, \alpha_k)$ and $RR(r_i, \mu_j, \alpha_k)$ are the numbers of galaxy-galaxy, galaxy-random and random-random pairs in bins centered on r_i , μ_j and α_k . The P_ℓ are the ℓ^{th} Legendre momenta.

The measurements of $\hat{\xi}_\ell(r)$ from all LRGs in our catalog, together with theoretical predictions of spatially-flat Λ CDM model with $\Omega_m = 0.25$ are shown on Fig. 2. Note that, Fig. 2 shows only statistical errors and does not show systematic errors on large scales (for details on systematic errors see Sec. 2.3). Also the statistical errors are computed from diagonal elements of the covariance matrix only, the whole structure of the covariance matrix is such that measurements are more likely to be systematically above or below theoretical line rather than randomly scattered around the theoretical prediction as for noncorrelated Gaussian variables.

RSD measurements are also often extracted from the normalised quadrupole $Q(r)$ (Hamilton 1992), defined as

$$Q(r) = \frac{\xi_2(r)}{\xi_0(r) - \frac{3}{r^3} \int_0^r \xi_0(r') r'^2 dr'}. \quad (5)$$

We can form an estimator for $Q(r)$ by replacing integral in Eq. (5) by a discreet sum

$$\hat{Q}(r_i) = \frac{\hat{\xi}_2(r_i)}{\hat{\xi}_0(r_i) - \frac{3}{r_i^3} \sum_{j=0}^{j \leq i} \hat{\xi}_0(r_j) r_j^2 \Delta r_j}. \quad (6)$$

The measured $Q(r)$ from the SDSS DR7 LRG data is shown in Fig. 3. The details of how the statistical error bars are computed are discussed in Sec. 3.7.

2.3 Modelling the redshift distribution of SDSS LRGs

To measure a correlation function from a survey accurately, we must know what an unclustered distribution of galaxies would look like in the same volume. The unclustered distribution can in principle be derived by averaging observations in many unconnected regions. Since the real data covers only a relatively small volume the expected galaxy density (in the absence of clustering) is hard to determine in this way (cosmic variance). The wrong estimate of unclustered distribution will bias the measurements of correlation function. The relative effect is especially important on large scales where the fluctuations we wish to measure are small.

In this paper we compute correlation function by using a spline fit to the galaxy redshift distribution (with parameters as given in Percival et al. 2010). We will refer to it as a “spline” random catalog. The exact form of the random catalog will depend on the position and number of nodes used for the spline. In the limiting case when the number of nodes goes to infinity while the spacing between nodes goes to zero we will have a random catalog that has exactly the same redshift distribution of galaxies as data. We refer to it as a “shuffled” catalog and construct it by randomly mixing angular positions and redshifts of galaxies in real catalog. We should expect this to remove some structure, as fluctuations in the galaxy density caused by large-scale structure will be smoothed.

To quantify the possible systematic offset induced by improper modelling of the radial distribution of galaxies we use large suite of LasDamas N-body simulations (McBride et al. 2011) which are designed to replicate the observed geometry of the SDSS-II (for more details on LasDamas simulations and how we use them see Sec. 3.7). For the mock catalogs the unclustered redshift distribution of galaxies is known and we will refer to the random catalog based on this known distribution as a “proper” random catalog. We compute correlation function of mocks using the “proper”, the “spline” and the “shuffled” random catalogs. The radial distribution of galaxies in each of these random catalogs, for one LasDamas mock, is shown on Fig. 4.

Figure 4 shows that although the “spline” random catalog follows the general shape of the “proper” random catalog, it does not reproduce the real radial distribution of galaxies accurately. The induced systematic errors on measurements of ξ_0 and ξ_2 by using “spline” and “shuffled” catalogs with respect to the “proper” catalog, for the same LasDamas mock, are shown on Fig. 5 along with the statistical errors.

Figure 5 shows that although the relative errors when using splined catalogs are smaller on smaller scales, they are comparable to current statistical errors on all scales. The statistical errors are larger for ξ_2 compared to ξ_0 . This is not surprising since the errors in redshift distribution effect clustering mainly in radial direction. ξ_0 measures average clustering in all direction, while ξ_2 measures the excess of clustering across the line-of-sight compared to radial and is expected to be affected by this systematics more. The differences between systematic errors induced by “spline” and “shuffled” catalogs are small; this shows that, unless the number of redshift nodes used for splining is very small, the exact nature of the distribution of nodes is not relevant.

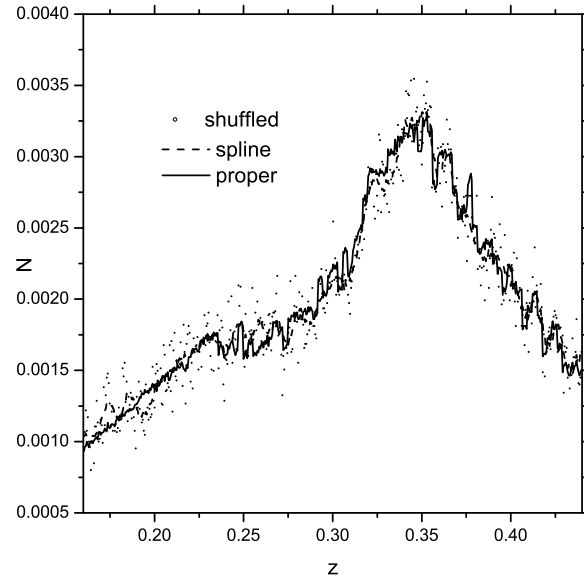


Figure 4. Radial distribution of galaxies in different random catalogs. Dashed line corresponds to the “shuffled” random catalog, which has radial distribution identical to that of data. Dashed line corresponds to “spline” random catalog and solid line corresponds to “proper” random catalog.

We see the similar consistent picture for all mock catalogs that are available to us. The systematic errors are on average comparable to the statistical errors on all scales. To account for this fact we rescale our statistical covariance matrix by a factor of two for all scales. This is a conservative assumption and for next generation of surveys, with significantly smaller statistical errors, a more accurate treatment will be required.

2.4 Excess of power on large scales

The top panel of Fig. 2 shows that there is an excess of power in the measured monopole of the correlation function with respect to the predictions of flat Λ CDM model. This excess has been observed previously in spectroscopic (Kazin et al. 2010) and photometric (Thomas et al. 2010) SDSS-II data sets. Thomas et al. (2010) assessed the extra power to be incompatible with the standard model at 4σ confidence level in the redshift range $0.45 < z < 0.65$. The effect is extremely unlikely to be due to cosmic variance, since the probability that the volume as large as the one surveyed by SDSS-II happened, by chance, to be significantly overdense compared to the average is minuscule (within the framework of the standard cosmological model).

If the signal is physical, the modifications to the standard cosmological model that result in stronger clustering, such as some modified gravity theories or clustering dark energy (Takada 2006), could explain this anomaly. Other possible explanations are the presence of large non-Gaussian initial conditions (Dalal et al. 2008) or isocurvature perturbations. Possible observational systematics include, for instance, improper modelling of extinction and seeing. Both of these could introduce spurious extra angular fluctuations in

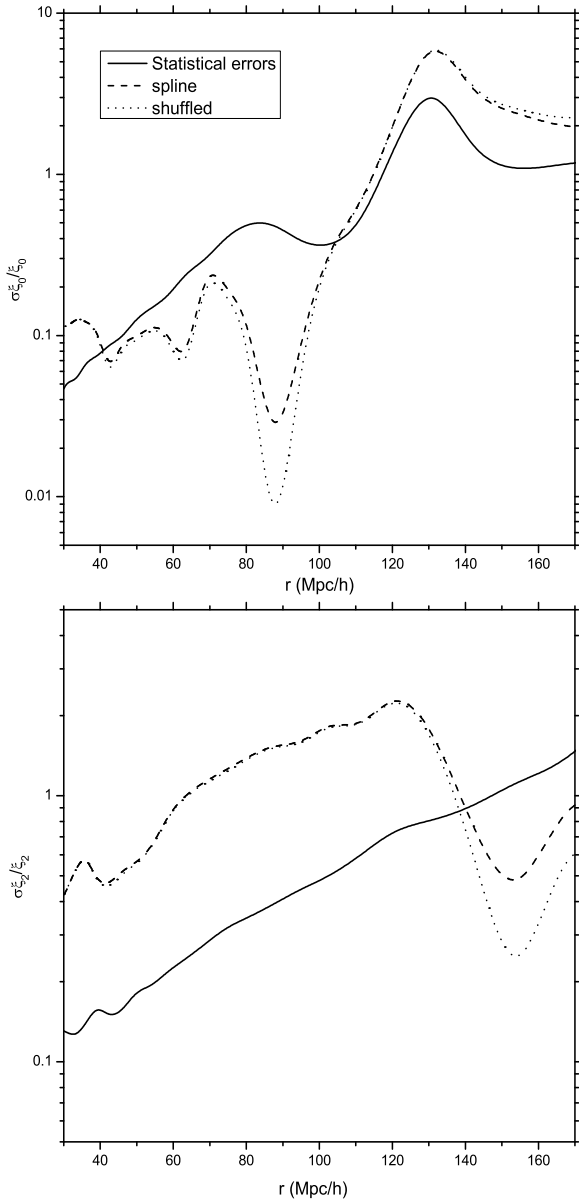


Figure 5. Dashed and dotted lines show relative errors introduced in the measurement of the first two even Legendre moments of the correlation function using “spline” and “shuffled” catalogs respectively. The solid line shows statistical errors.

the data that would later be misinterpreted as an excess of power. Inaccuracies in the measured clustering induced by assuming an incorrect radial distribution, are also large and could in principle explain the anomaly (Kazin et al. 2010). The error rescaling suggested in previous section makes the inconsistency with the standard model on very large scales less severe.¹

¹ Also note that the measurements of spherically averaged correlation function at different scales are strongly correlated. This makes the deviations to the one side of the model prediction more probable, the significance of this deviation being smaller than what it would be for uncorrelated measurements.

3 MODELING RSD ON LARGE SCALES

3.1 Plane-Parallel, Linear model

The linear, plane-parallel model for RSD is often termed the Kaiser model (Kaiser 1987). In the following, we follow standard convention and denote the observed galaxy overdensity field by δ_g , with a superscript s in redshift-space and r in real-space. A given Fourier k mode of this overdensity can be expressed to linear order in overdensity as

$$\delta_g^s(k) = \delta_g^r(k) - \mu^2 \theta_g(k), \quad (7)$$

where μ is the cosine of an angle with respect to the line of sight and $\theta_g = \nabla \cdot u$ is a divergence of the galaxy velocity field. We follow the commonly adopted assumption that this is equal to the divergence of the matter field, assuming no velocity bias. i.e.. we assume that $b_v(k) = 1$, where $\theta_g(k) = b_v(k)\theta_m(k)$. A subscript g shows that a quantity relates to the galaxy field, and a subscript m denotes the matter field.

The two-point function of this overdensity field is anisotropic,

$$P_{gg}^s(k) = P_{gg}^r(k) - 2\mu^2 P_{g\theta}^r(k) + \mu^4 P_{\theta\theta}^r(k), \quad (8)$$

where $P_{xy} = \langle \delta_x \delta_y \rangle$ denotes a cross-power-spectrum of fields x and y . The redshift-space correlation function is given by the Fourier transform of Eq. (8)

$$\xi_{gg}(r, \mu) = \int P_{gg}(k, \mu) \exp(-i\mathbf{k}\mathbf{r}) d^3k, \quad (9)$$

and can also be expressed in terms of its Legendre momenta (Hamilton 1992, 1997).

If we further assume that, in real-space, the overdensities in the galaxy field are linear functions of overdensities in the matter field $\delta_g = b\delta_m$ and the velocity divergence can be related to the matter overdensities using the linearized continuity equation $\delta_\theta = -f\delta_m$, then the redshift-space power-spectrum can be simply expressed in terms of the real-space power-spectrum as

$$P_{gg}^s(k, \mu) = (b + f\mu^2)^2 P_{mm}^r(k). \quad (10)$$

The proportionality constant b between matter and galaxy overdensities is the bias factor and the coefficient f between velocity divergence and the matter overdensity is equal to the logarithmic derivative of the growth factor by a scale factor $d \ln G / d \ln a$, which follows from the continuity equation combined with scale-independent growth.

3.2 Wide-angle effects

When the distance between galaxy pairs is comparable to the distance between galaxies and the observer, the theory of Sec. 3.1 can not be used to describe RSD effects. The redshift-space correlation function becomes a function of three variables that can be chosen to be the separation between galaxies r and the two angles ϕ_1 and ϕ_2 that galaxies form with an arbitrary z axis with respect to the observer (Zaroubi & Hoffman 1993; Szalay et al. 1998; Szapudi 2004). Papai & Szapudi (2008) showed that this correlation function, when expanded in tripolar spherical harmonics,

$$\xi_s(r, \phi_1, \phi_2) = \sum_{\ell_1, \ell_2, \ell} B^{\ell_1, \ell_2, \ell}(r, \phi_1, \phi_2) S_{\ell_1, \ell_2, \ell}(\hat{\mathbf{x}}_1, \hat{\mathbf{x}}_2, \hat{\mathbf{x}}), \quad (11)$$

gives only a few non-zero terms in the absence of an observational window. Here $\hat{\mathbf{x}}_1$ and $\hat{\mathbf{x}}_2$ are the unit vectors in the direction of two galaxies and $\hat{\mathbf{x}}$ is a unit vector pointing in the direction from galaxy one to galaxy two.

Eq. (11) can be recast as a function of variables r , μ and α , where α is an angle the galaxies make with respect to the observer. This set of coordinates is invariant with respect to rotation and more straightforward to use in data analysis. There are three reasons for differences between “plane-parallel” and “wide-angle” predictions:

- (a) The “wide-angle” correlation function $\xi(r, \mu, \alpha)$ depends on α , while the “plane-parallel” one doesn’t;
- (b) The coefficients $B^{\ell_1, \ell_2, \ell}$ depend on the density of galaxies $n(z)$ as a function of redshift. This implies that the RSD effect will depend on the spatial distribution of observed galaxies;
- (c) The distribution of galaxies in μ will be non-trivial, with some values of μ not permitted for non-zero α . As a consequence, we will not be able to measure pure Legendre momenta of the correlation function, but instead will use weighted integrals and biased momenta.

In Raccanelli et al. (2010) we used simulations to demonstrate these effects, showing that they should be carefully taken into consideration in order to fit the measured wide-angle correlation function. In the following we describe (a) and (b) as wide-angle effects, whereas (c) is termed the “ μ -distribution” as it could be applied to plane-parallel and wide-angle theory of individual line-of-sight.

Allowing for full distribution of galaxy pairs, the estimates of Legendre momenta given by Eq. (4) correspond to

$$\xi_\ell(r) = \int \xi(r, \mu, \alpha) W(r, \mu, \alpha) P_\ell(\mu) d\mu d\alpha, \quad (12)$$

where $\xi(r, \mu, \alpha)$ is given by either the wide-angle formula in Eq. (11) or its plane-parallel equivalent computed from Eq. (10). $W(r, \mu, \alpha)$ is a weight factor that gives the relative number of pairs in a survey that form angles μ and α for a given scale r . The weight factor W is normalised so that

$$\int W(r, \mu, \alpha) d\mu d\alpha = 1 \quad (13)$$

for all scales r . Ignoring (a) corresponds to setting $W(r, \mu, \alpha \neq 0) = 0$ and ignoring (c) corresponds to setting $W(r, \mu, \alpha) = 1$.

Fig. 6 shows the normalized distribution of pairs in μ and α for different scales for the SDSS DR7 LRG catalog. When the α distribution tends towards a delta function centred at $\alpha = 0$, the wide-angle effects (a) becomes negligible. When μ tends towards a uniform distribution, (c) becomes negligible. In general, the relative importance of the wide-angle effects on the measured correlation function depends on the geometry of the survey, its redshift range and what scales are considered. The effect is stronger for lower redshifts and becomes increasingly important on larger scales. In Sec. 3.7 we will show that for the SDSS DR7 geometry the difference due to (a) and (b) in the list above are much smaller than statistical errors and can be safely ignored even for scales as large as $200 h^{-1}$ Mpc, while the differences due to nontrivial μ -distribution (item (c) in the list above) are

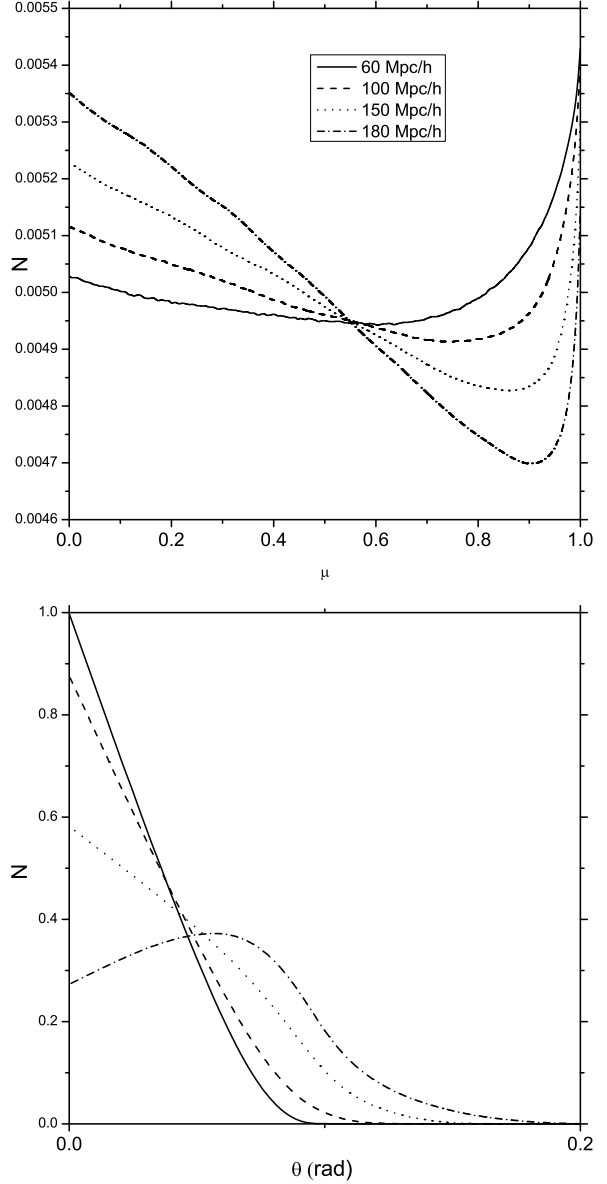


Figure 6. Normalised distribution of pairs in SDSS DR7 LRG catalog as a function of μ and α at different scales.

comparable to statistical errors and need to be taken into account.

3.3 Nonlinear effects

The following nonlinear effects, if they are comparable to the measurement errors, can make Eq. (10) unsuitable for analysing RSD data

(a) Nonlinear contributions to the relationship between matter and galaxy overdensities $\delta_g^r = h(\delta_m^r)$, where h is an arbitrary function.

(b) The relationship between the velocity divergence and matter overdensities $\theta_g = -f\delta_m$ relies on scale-independent linear growth coupled with the continuity equation. This formula will break down if these conditions are not met.

(c) The matter power spectrum itself goes non-linear, because of the scale-dependent non-linear growth on smaller scales.

(d) The real-space to redshift-space mapping includes higher order terms involving δ_g^r and θ_g

In the following, we are only interested in the signal on large-scales where linear theory should be strongest. We therefore assume that all non-linear effects are small except for (c), where we allow the overall power spectrum shape to deviate from the linear form. We use mock catalogues in Section 3.7 to confirm the validity of this assumption.

In order to approximate the non-linear power spectrum, we adopt a two-component model, which splits $P(k)$ into a “smooth” part that describes the overall shape and a “wiggled” part that describes the Baryon Acoustic Oscillations (BAO),

$$P_{\text{bao}}(k, \mu) = P_{\text{full}}(k, \mu) - P_{\text{smooth}}(k, \mu) \quad (14)$$

The “smooth” part is defined by taking some reasonably spaced points k_i (we adopt the node spacing of Percival et al. 2010) and then interpolating the power spectrum values between those nodes using a bi-cubic spline interpolation routine (Press et al. 1992).

The primary non-linear effect on the BAO component of the power spectrum is a damping on small scales, which can be well approximated by a Gaussian smoothing (Bharadwaj 1996; Crocce & Scoccimarro 2006, 2008; Eisenstein et al. 2007; Matsubara 2008a,b)

$$P_{\text{bao}}^{\text{nl}}(k, \mu) = P_{\text{bao}}^{\text{lin}}(k, \mu) \times \exp \left(-k^2 \left[\frac{(1 - \mu^2)\Sigma_{\perp}}{2} + \frac{\mu^2\Sigma_{\parallel}}{2} \right] \right), \quad (15)$$

where $\Sigma_{\perp} = \Sigma_0 G$ and $\Sigma_{\parallel} = \Sigma_0 G(1 + f)$. Σ_0 is a constant phenomenologically describing the nonlinear diffusion of the BAO peak due to nonlinear evolution. From N-body simulations its numerical value is of order $10 h^{-1} \text{Mpc}$ and seems to depend linearly on σ_8 but only weakly on k and cosmological parameters.

3.4 Fingers of god effect

Within dark matter haloes the peculiar velocities of galaxies are highly non-linear. These velocities can induce RSD that are larger than the real-space distance between galaxies within the halo. This gives rise to the observed fingers of god (FOG) effect – strong elongation of structures along the line of sight (Jackson 1972). The FOG effect gives a sharp reduction of the power spectrum on small scales compared to the predictions of the linear model, and is usually modeled by multiplying the linear power-spectrum by a function $F(\sigma_v, k, \mu)$, where σ_v is the average velocity dispersion of galaxies within the relevant haloes. The function F is chosen so that it is small on small scales and approaches unity for scales larger than $1/\sigma_v$. The two most frequently used functions are (e.g. Cole et al. 1995; Peacock & Dodds 1996)

$$F_{\text{Lorentzian}}(k, \mu^2) = [1 + (k\sigma_v\mu)^2]^{-1}, \quad (16)$$

$$F_{\text{Gaussian}}(k, \mu^2) = \exp[-(k\sigma_v\mu)^2]. \quad (17)$$

Note that this model is constructed by a rather ad-hoc splicing of the FOG signal together with the linear model and

ignores the scale-dependence of the mapping between real and redshift-space separations (Fisher 1995; Scoccimarro 2004, and references therein). In addition, the exact form of $F(k, \mu^2)$, and the value of σ_v is strongly dependent on the galaxy population (Jing & Börner 2004; Li et al. 2007).

3.5 Degeneracy with Alcock-Paczynski effect

The positions of galaxies in our catalog are given in terms of the angular positions and redshifts. To convert angular and redshift separations into physical distances the angular and radial distances as functions of redshift are required. Those functions depend on the adopted cosmological model. We perform our pair count assuming a fiducial, spatially-flat cosmology with $\Omega_m = 0.25$. If the real cosmology is significantly different from the fiducial one, this difference will introduce additional anisotropies in the correlation function through the Alcock-Paczynski (AP) effect (Alcock & Paczynski 1979). This can significantly bias the measurements of growth (Ballinger et al. 1996; Simpson & Peacock 2010; Samushia et al. 2010).

In the presence of Alcock-Paczynski effect the redshift-space power-spectrum is

$$P^s(k', \mu', \alpha_{\perp}, \alpha_{\parallel}, \mathbf{p}) = \left(b + \frac{\mu'^2 f}{F^2 + \mu'^2(1 - F^2)} \right)^2 \alpha_{\perp}^{-2} \alpha_{\parallel}^{-1} \times P^r \left(\frac{k'}{\alpha_{\perp}} \sqrt{1 + \mu'^2 \left(\frac{1}{F^2} - 1 \right)} \right), \quad (18)$$

where \mathbf{p} are standard cosmological parameters determining the shape of the real-space power-spectrum, k' and μ' are the observed wavevector and angle, related to the real quantities by

$$k'_{\parallel} = \alpha_{\parallel} k_{\parallel}, \quad (19)$$

$$k'_{\perp} = \alpha_{\perp} k_{\perp}, \quad (20)$$

$$\mu' = \frac{k'_{\parallel}}{\sqrt{k'^2_{\parallel} + k'^2_{\perp}}}, \quad (21)$$

the α_{\parallel} and α_{\perp} are the ratios of angular and radial distances between fiducial and real cosmologies

$$\alpha_{\parallel} = \frac{H^{\text{fid}}}{H^{\text{real}}}, \quad (22)$$

$$\alpha_{\perp} = \frac{D^{\text{real}}}{D^{\text{fid}}}, \quad (23)$$

and $F = \alpha_{\parallel}/\alpha_{\perp}$.

Ignoring the AP effect is equivalent to assuming that α factors are equal to unity in Eq. (18). This assumption can bias estimates of growth parameters and their uncertainties.

We estimate to magnitude of this effect for our analysis using Fisher matrix method. We compute a Fisher matrix for the SDSS-II like survey following Samushia et al. (2010). This Fisher matrix is an optimistic estimate of the inverse covariance matrix on the parameters b , f , α_{\parallel} , α_{\perp} and \mathbf{p} . The covariance matrix is an inverse of this fisher matrix. Ignoring the Alcock-Paczynski effect is equivalent to removing rows and columns corresponding to α_{\parallel} and α_{\perp} first, as if they were perfectly known, and only then inverting the fisher matrix to get covariance of b and f . The more accurate approach is to invert the Fisher matrix directly without assuming that the α -s are known.

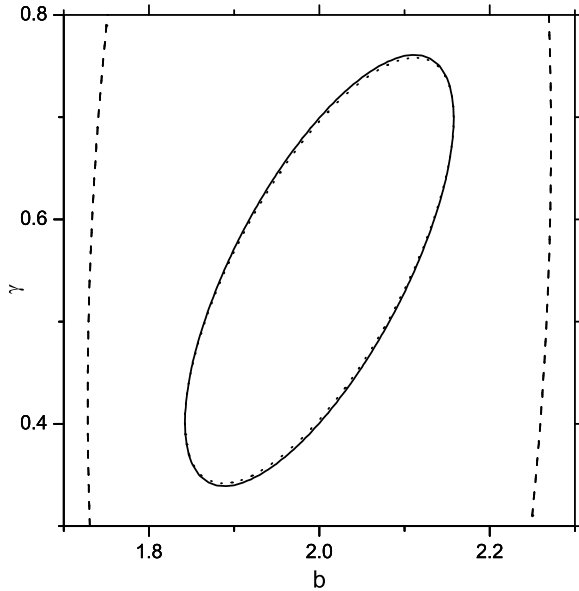


Figure 7. Fisher matrix predictions of correlated constraints on parameters b and γ from a SDSS-II like survey. The dashed contours correspond to the most general case when the AP effect is not ignored, the dotted lines correspond to the case when the AP effect is ignored and the solid lines correspond to the case when the AP effect is ignored but a strong prior is put on the background cosmology. The solid and dotted lines are almost indistinguishable by eye on this plot.

In our data analysis, we will apply a prior based on the WMAP and SNIa data on the background geometry of the Universe (see Sec. 4). To reflect this in our Fisher matrix computations we first add this prior to the Fisher matrix elements corresponding to α_{\parallel} and α_{\perp} and only then invert the whole matrix to get covariances on b and f . We compare the result with the resulting covariances when the AP effect is ignored.

On Figs. 7 and 8 we show the effects of AP on the measurements of different growth parameters (for the description of parameters γ and f see Sec. 4). These figures show that in general ignoring the AP effect results in gross underestimation of the error bars. Real uncertainties on γ and f are few times larger than what we would get when ignoring AP. After applying the strong prior on the background expansion, however, almost all of this degeneracy is removed and the uncertainties in the measurements of growth and bias are almost identical to the case with no AP, consistent with the work of Samushia et al. (2010), which showed the importance of model assumptions on this measurement. We conclude that, for the models we test, the effects of the degeneracy between RSD and AP on the error bars of our measurements are very small and can be safely ignored.

3.6 Summary of RSD models

We now consider the relative importance of the modifications to the linear plane-parallel model, described in previous subsections, as a function of scale. We have done this for a spatially-flat Λ CDM model with $\Omega_m = 0.25$: Figs. 9 and 10 compare statistical errors on measurements of $\xi_{\ell}(r)$

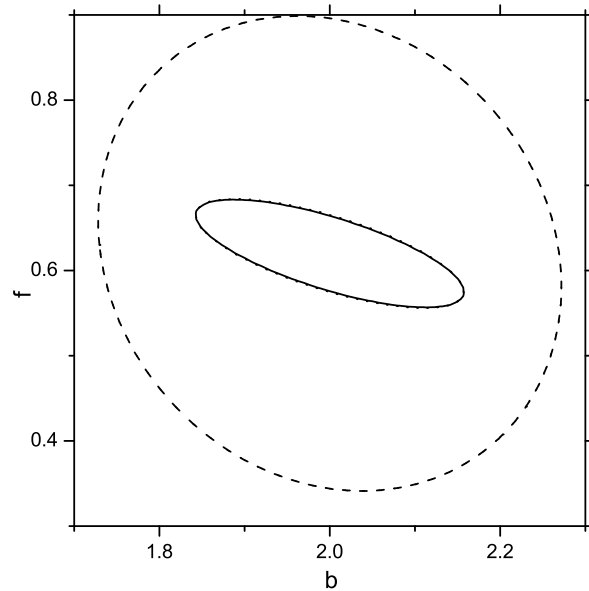


Figure 8. Fisher matrix predictions of correlated constraints on parameters b and f from a SDSS-II like survey. The dashed contours correspond to the most general case when the AP effect is not ignored, the dotted lines correspond to the case when the AP effect is ignored and the solid lines correspond to the case when the AP effect is ignored but a strong prior is put on the background cosmology. The solid and dotted lines are almost indistinguishable by eye on this plot.

and $Q(r)$ (for the details of how these statistical errors are estimated see Sec. 3.7) with the differences in theoretical models induced by modifications considered above.

To estimate the impact of different systematics we first compute a theoretical correlation function for our fiducial model $\xi(\mathbf{r})^{\text{full}}$ including all effects. We compute linear $\xi(\mathbf{r})$ using CAMB (Lewis, Challinor & Lasenby 2000). Then we recompute the same correlation function by ignoring each of the systematic effects in turn to see by how much this changes our theoretical estimates at different scales. Nonlinear diffusion of the BAO peak is modelled with the Eq. (15) with $\Sigma_0 = 8 h^{-1}$ Mpc; the FOG effect with the Gaussian damping function of Eq. (17) with $\sigma_v = 3.5 h^{-1}$ Mpc; the effect of μ distribution is studied first by using the real distribution of angles in SDSS geometry for W and then assuming it to have a uniform probability over all angles; the small scale nonlinearities are modelled with the HALOFIT fitting formula of Smith et al. (2003); the wide-angle effects are estimated by substituting the full wide-angle correlation function by a two-dimensional plane-parallel one.

The results are shown on Figs. 9 and 10. The FOG effect and corrections to the shape of the correlation function due to nonlinear growth of structure are only important on smaller scales and become significantly smaller than the measurement errors on the scales larger than $20 h^{-1}$ Mpc. The wide angle effects appear at the scales of about $70 h^{-1}$ Mpc, as anticipated based on Fig. 6, but are less than 1 percent even on the scales as large as $200 h^{-1}$ Mpc. The effects of nonlinear BAO diffusion and non-isotropic μ -distribution become comparable to the error-bars on scales between $80 h^{-1}$ Mpc and $200 h^{-1}$ Mpc and should be taken

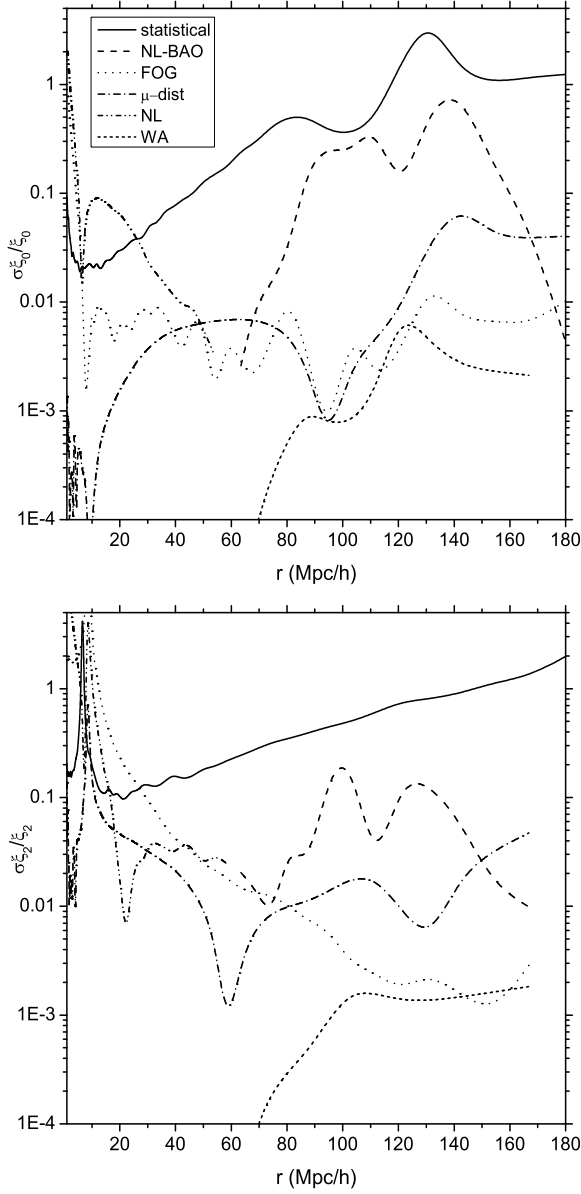


Figure 9. Relative impact of nonlinear and wide-angle effects compared to the statistical errors on the measurements of $\xi_\ell(r)$ from SDSS DR7 data.

into account to get accurate theoretical predictions. In what follows we will therefore only use the data on scales between $30 h^{-1} \text{ Mpc}$ and $200 h^{-1} \text{ Mpc}$, and will ignore the nonlinear FOG, nonlinear growth other than BAO diffusion and wide-angle effects, but will take into account the effects of nonlinear BAO diffusion and the μ distribution.

In Sec. 3.7 we test the applicability of our model on the mock catalogs. The measurements of mean ξ_ℓ from the mocks have statistical error bars that are approximately nine times smaller compared to the SDSS data. To fit the mock measurements accurately we will also have to take into account the FOG effect.

To summarise, our theoretical model of the correlation function will be given by

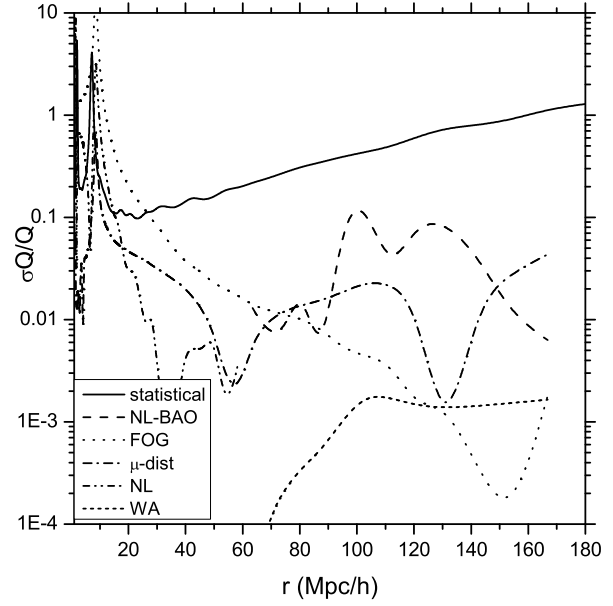


Figure 10. Relative impact of nonlinear and wide-angle effects compared to the statistical errors on the measurements of $Q(r)$ from SDSS DR7 data.

$$\xi_\ell(r)^{\text{th}} = \int \xi^{\text{th}}(r, \mu, \alpha) W(r, \mu, \alpha) P_\ell(\mu) d\mu d\alpha, \quad (24)$$

where the function $\xi^{\text{th}}(r, \mu, \alpha)$ is computed by Fourier transforming a power-spectrum given by formula in Eq. (10). We will model the real-space power-spectrum on the right hand side of Eq. (10) as a linear power-spectrum damped with a Gaussian function of Eq. (15) to account for nonlinear diffusion of the BAO peak.

3.7 Testing RSD models with mock catalogs

To test our analysis of the effects that have to be taken into account to analyse RSD in SDSS DR7 data, and to estimate the statistical errors on our measurements (as shown on Fig. 2), we use galaxy catalogs from the Large Suite of Dark Energy Simulations (LasDamas: McBride et al. 2011)². The LasDamas simulations are designed to model the clustering of Sloan Digital Sky Survey (SDSS) galaxies in a wide luminosity range and in the redshift range $0.16 < z < 0.44$. The simulations are produced by placing artificial galaxies inside dark matter halos using an HOD with parameters measured from the respective SDSS galaxy samples. We use 80 “Oriana” catalogs that have exactly the same angular mask as the SDSS survey and subsample them to match the redshift distribution of the Luminous Red Galaxies (LRG) in our SDSS DR7 data set. The LasDamas mocks have insufficient galaxies at redshifts below $z < 0.2$, a region that we ignore as it contains only a small fraction of the volume available.

We apply exactly the same weighting to the mocks as to the real catalog and compute zeroth, second and fourth Legendre momenta of the redshift-space correlation function from them using Eq. (4). We also compute the normalised quadrupole $Q(r)$ as given by Eq. (6).

² <http://lss.phy.vanderbilt.edu/lasdamas/>

We estimate covariance matrices corresponding to the statistical errors of our measurements, based on assuming that the Legendre momenta are drawn from a multi-variate Gaussian distribution

$$\mathbf{C}^{\text{stat}} = \frac{1}{79} \sum [\hat{\mathbf{X}}(r_i) - \bar{\mathbf{X}}(r_i)] [\hat{\mathbf{X}}(r_j) - \bar{\mathbf{X}}(r_j)], \quad (25)$$

where $\hat{\mathbf{X}}(r)$ is a vector of the measurements of ξ_ℓ at scale r for $\ell = 0, 2, 4$ and $\bar{\mathbf{X}}$ is the mean value from all 80 mock catalogs.

The mean Legendre momenta measured from the LasDamas mocks are shown in Fig. 11. The error-bars correspond to the square root of the diagonal terms in the covariance matrix $\mathbf{C}^{\text{stat}}/80$ and the lines show theoretical predictions computed making different assumptions. Our theoretical predictions, with the parameters of the simulations, provide a very good fit to the data. The bottom panel on Fig. 11 shows that the theoretical prediction underestimates ξ_4 on scales smaller than $50 h^{-1}$ Mpc. The fourth Legendre moment measures a higher frequency μ dependence of correlation functions and therefore is more sensitive to different systematic effects. Since we are not using $\xi_4(r)$ in our fits we did not attempt to investigate this issue further. The measurements are strongly positively correlated and the error-bars presented here reflect only small part of the covariance matrix.

Fig. 12 shows the measurements of Q from LasDamas mocks with the similar definition of the error-bars as Fig. 11. In the Kaiser formalism $Q(r)$ is expected to be a straight line damped at smaller scales because of FOG effects. In reality the measured $Q(r)$ will deviate from a straight line even within the Kaiser model at larger scales since it is estimated by a discrete sum in Eq. (6) instead of continuous integral. Figs. 11 and 12 clearly show that the model adopted in Sec. 3.6 can describe the measurements very well on all scales between $30 h^{-1}$ Mpc and $200 h^{-1}$ Mpc, while using the Kaiser formula without modifications would fail to fit on scales around BAO peak and larger.

4 TESTING COSMOLOGICAL MODELS

Figure 2 shows that the signal to noise of the measured ξ_4 is very small on all scales so that it can not be used to extract RSD information. Consequently, for simplicity, we will not include measurements of ξ_4 in our analysis.

The normalised quadrupole Q by definition does not contain any extra information compared to ξ_0 and ξ_2 . Figure 10 shows that our measurements of Q are noisier than first two Legendre momenta on scales larger than $50 h^{-1}$ Mpc. The analysis of Q measurements is in some way simpler, because the normalised quadrupole, under some general assumptions,³ does not depend on the shape of the power spectrum and only depends on the parameters describing the amplitude. The drawback is that with Q only a combination of growth and bias $\beta = f/b$ can be measured, but not the two parameters individually.

In our analysis we will perform a joint fit to ξ_0 and ξ_2 instead of fitting Q . We will explicitly use a prior based

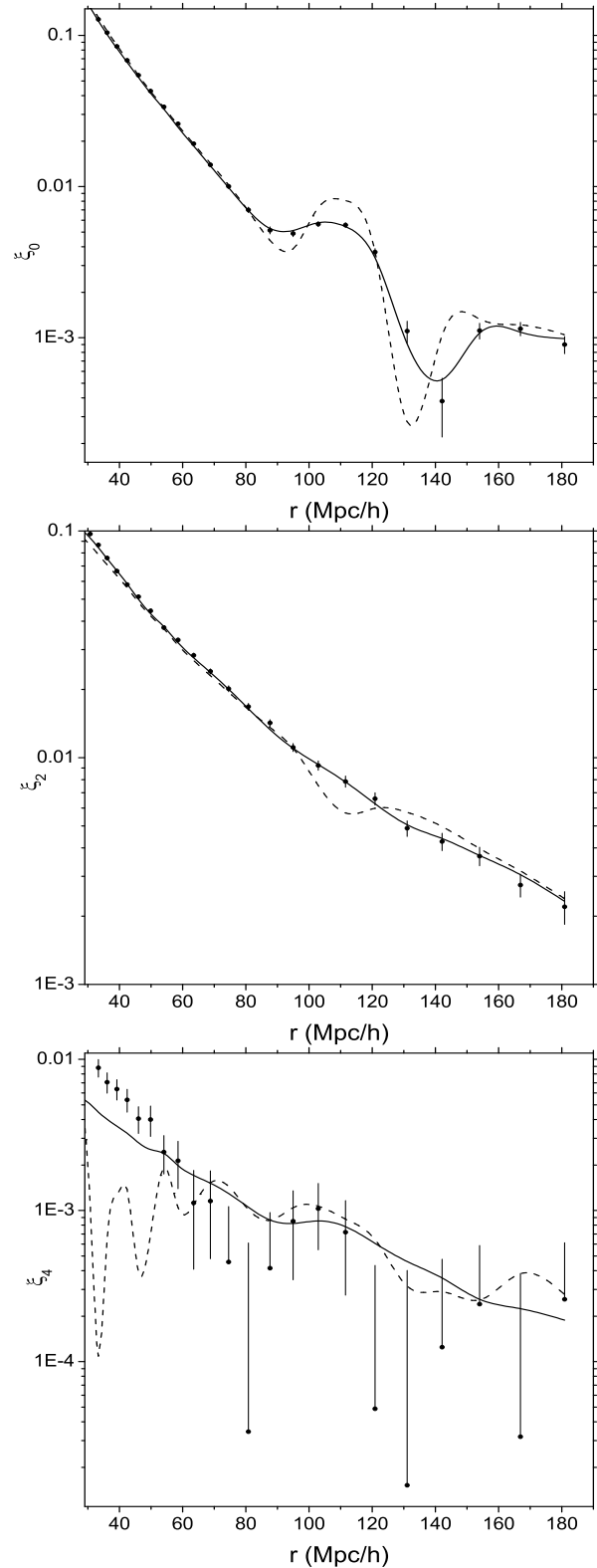


Figure 11. Measurements of mean ξ_ℓ from 80 LasDamas “Orion” mocks in a redshift range $0.16 < z < 0.44$. Dashed line shows predictions of the Kaiser model, while solid line corresponds to the theoretical predictions of our model.

³ This does not hold, for example, when the μ distribution does not correspond to an isotropic distribution of galaxy pairs.

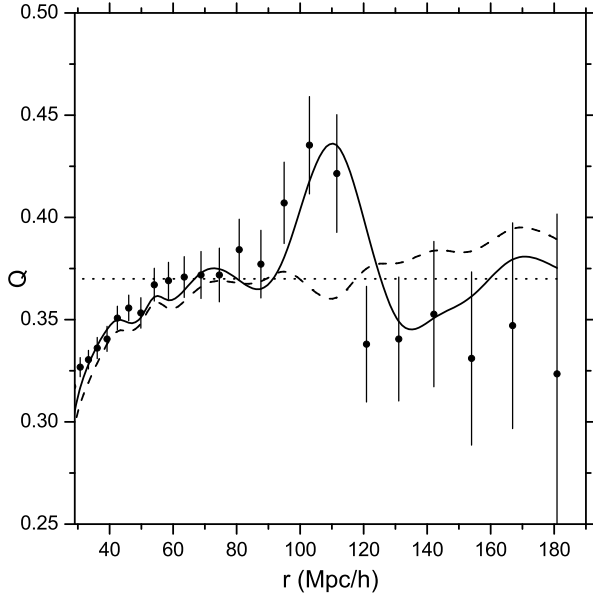


Figure 12. Measurements of mean Q from 80 LasDamas “Oriana” mocks in a redshift range $0.16 < z < 0.44$. Dotted line shows theoretical predictions of Kaiser model, dashed line shows predictions of the Kaiser model with FOG corrections and accounting for the fact that Q is computed from a discrete sum, while solid line corresponds to the theoretical predictions of our model.

on the joint constraints from WMAP and SNIa data to deal with the ambiguity in the shape of the matter power-spectrum. This will allow us to measure bias and growth at the same time and to extract more information from the correlation function. From the analysis presented in Section 3, and especially Figs. 9 & 10, we see that we would have to make the same level of corrections to the linear plane-parallel model for Q as we would do for a joint fit (see also Tocchini-Valentini et al. 2011).

We will fit models to the first two even Legendre momenta of correlation function instead of fitting to the two dimensional correlation function $\xi(\mathbf{r})$. We do this for two reasons: a pair of one-dimensional functions ξ_0 and ξ_2 are easier to visualise and work with and, as we showed above, they contain most of the cosmologically relevant information anyway; also the measurement errors on ξ_ℓ are more Gaussian, as we show in Sec. 4.2 compared to the errors of $\xi(\mathbf{r})$ and therefore the reconstruction of the likelihood surfaces is more robust.

Our theoretical model of Legendre momenta of the correlation function will depend on a set of parameters \mathbf{p} describing background expansion of the Universe and a set of parameters $\mathbf{A}(z)$ describing the amplitude of the correlation function and its growth with redshift. Each model will also depend on the phenomenological parameter Σ_0 describing nonlinear diffusion of the BAO peak. We will treat Σ_0 as a nuisance parameter and marginalise over it with a uniform prior. For this reason, we do not include the Σ_0 dependence of the likelihood in the equations given below.

For the background expansion we will assume that the Universe is well described by a spatially-flat Λ CDM model composed of non-relativistic matter with energy density Ω_m some part of which is in baryons with energy density Ω_b .

The rest of the energy density, in this model, is assumed to be in a smooth dark fluid with the equation of state w . To complete the background model we need to specify the expansion rate of the Universe at present $h = H_0/100$, where H_0 is a Hubble parameter.

For the cosmological parameters describing the observed amplitude of clustering we will make three different assumptions ranging from the most specific model to more general assumptions.

For every theoretical model we compute a χ^2 function

$$\chi_{\text{tot}}^2(\mathbf{p}, \mathbf{A}) = [\hat{\mathbf{X}} - \mathbf{X}(r_i)] \mathbf{C}_{\text{tot}} [\hat{\mathbf{X}} - \mathbf{X}(r_j)]^T, \quad (26)$$

where $\hat{\mathbf{X}}(r)$ is a vector of the measured $\xi_0(r)$ and $\xi_2(r)$, $\mathbf{X}(r)$ is the model to be tested, and the total covariance matrix is given by

$$\mathbf{C}_{\text{tot}} = 2 * \mathbf{C}^{\text{stat}}. \quad (27)$$

Assuming that the measurement errors are closed to Gaussian, the likelihood for a given set of cosmological parameters given data will be

$$\mathcal{L}_{\text{tot}} = \exp(-\chi_{\text{tot}}^2/2). \quad (28)$$

4.1 Inaccuracies in the estimation of covariance matrix

Estimating covariance matrices of galaxy two-point correlation function in configuration space is a nontrivial task. Many different techniques have been used before to tackle this issue, including internal procedures – based only on the observed data itself – such as jackknife (Lucey 1979) and bootstrap (Barrow et al. 1984) methods; analytical estimates of the errors (Mo, Jing & Börner 1992); Monte-Carlo sampling of random initial conditions and combination of analytical methods and Monte-Carlo (Padmanabhan et al. 2005). Studying the three-dimensional clustering on scales below $25 h^{-1}$ Mpc, Norberg et al. (2009) showed that internal methods do recover the principal components of the real covariance matrix in a robust way but can not accurately reproduce the errors themselves, usually overestimating them by as much as 40 percent.

Our statistical covariance matrices are estimated from the sample of 80 mock catalogs. This number is far less than sufficient to accurately measure the errors and correlations. Cabré et al. (2008) used a sample of 1000 mocks, in their study of cross-correlation between the map of CMB temperature anisotropies and large scale structure, and found that even with 200 simulations the error bars could be underestimated by about 20 percent.

One of the ways of reducing the effect of inaccurate covariance matrix estimation is to find the eigenvectors of the normalized covariance matrix and then only use the eigenmodes that have high signal to noise, since there error estimates are expected to be more reliable. We do not attempt to do this in our paper; this would remove large scale information which we are interested in.

We will use the full covariance matrix estimated from 80 mock catalogs as our best guess to the real structure of the measurement errors. This is good enough for the purposes of our current work. As we will show below the errors on current data are too big to result in tight constraints on cosmological parameters and we apply our method to the

real SDSS-II data to provide a “proof of concept”. Next generation of surveys, with significantly tighter error bars on the measurements of correlation function, will require a more thorough investigation of this issue.

4.2 Inaccuracies in the posterior likelihood function

Equation (28) represents a true likelihood function only if the measurements of variables \mathbf{X} that were used in computing χ^2 have errors that are distributed as multivariate Gaussian random variables. There are reasons to believe that the errors on ξ_0 , for instance, are not Gaussian (Norberg et al. 2009). To check if the assumption of Gaussianity holds reasonably well for our measurements we take the measurements of ξ_0 and ξ_2 at the different scales from all 80 mock LasDamas catalogs and construct normalized variables

$$\mathbf{Y} = \frac{\hat{\mathbf{X}} - \bar{\mathbf{X}}}{\sigma_{\mathbf{X}}}, \quad (29)$$

where $\bar{\mathbf{X}}$ and $\sigma_{\mathbf{X}}$ are the average value and dispersion computed from all 80 mocks. If the measured $\hat{\mathbf{X}}$ are Gaussian, \mathbf{Y} should be distributed according to the normal distribution with mean zero and variance one.

Figs. 13 & 14 shows the distribution of \mathbf{Y} for the measurements of ξ_0 and ξ_2 .

We perform a Kolmogorov-Smirnov test to see if the empirical distribution of ξ_ℓ measurements is consistent with the null hypothesis that they are drawn from a Gaussian distribution. The Kolmogorov-Smirnov test confirms that the distribution of ξ_0 is consistent with the null hypothesis at 13 percent confidence level and ξ_2 is consistent at 25 percent confidence level. In both cases the small possible deviations from Gaussian cumulative distribution function reflect the fact that deviations above the mean value are slightly more likely than deviations below the mean at the tails of the distribution.

To check how the Gaussianity of ξ_ℓ measurement errors depends on the scale we split r range into two with $30 h^{-1} \text{ Mpc} < r_1 < 75 h^{-1} \text{ Mpc}$ and $75 h^{-1} \text{ Mpc} < r_2 < 200 h^{-1} \text{ Mpc}$ and perform a similar Kolmogorov-Smirnov test on small scale and large scale measurements separately. Our empirical distribution of ξ_0 is more consistent with the assumption of Gaussianity on small scales. For r_1 the KS test accepts the null hypothesis at 36 percent, while for r_2 the null hypothesis is accepted at 8 percent. For the ξ_2 the trend is opposite KS likelihood for r_1 is 5 percent, while for r_2 it is 17 percent.

The variable $\log(1 + \xi_0)$ is a slightly better fit to the assumption of Gaussianity, with a KS likelihood of 23 percent over all scales.

For our purposes the variables ξ_0 and ξ_2 are close enough to the Gaussian distributed variables and we conclude that the usage of Eq. (26) is justified for computing likelihood surfaces and confidence level intervals.

The two dimensional redshift-space correlation function $\xi(\sigma, \pi)$, where σ and π are along the line-of-sight and across the line-of-sight separations, itself is often used in the analysis of RSD and BAO. We perform the same check on the measurements of this two dimensional correlation function between the scales of $30\text{--}60 h^{-1} \text{ Mpc}$. The resulting histogram is shown on Fig. 15.

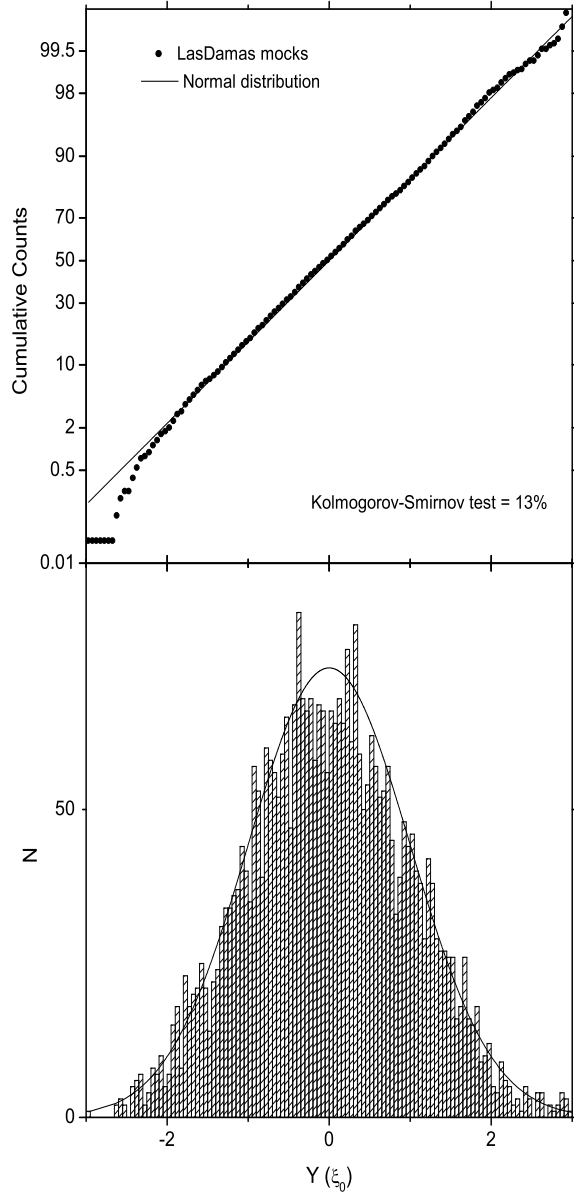


Figure 13. Histogram of the normalised scattering of ξ_0 measurements and their cumulative distribution from 80 mock LasDamas catalogs compared to the normal distribution with mean zero and unit variance.

Figure. 15 shows that the distribution of measured $\xi(\sigma, \pi)$ around its mean value, at least for the mock catalogs that we use, are not Gaussian. We conclude that if the χ^2 and likelihood functions are defined as in Eqs. (26) and (28), the Legendre momenta are more appropriate as variables compared to the two-dimensional correlation function. This is not surprising since the measured Legendre momenta are the weighted sums of the two-dimensional correlation function and will always tend to be more Gaussian irrespective of the underlying distribution, thanks to the Central Limit Theorem.

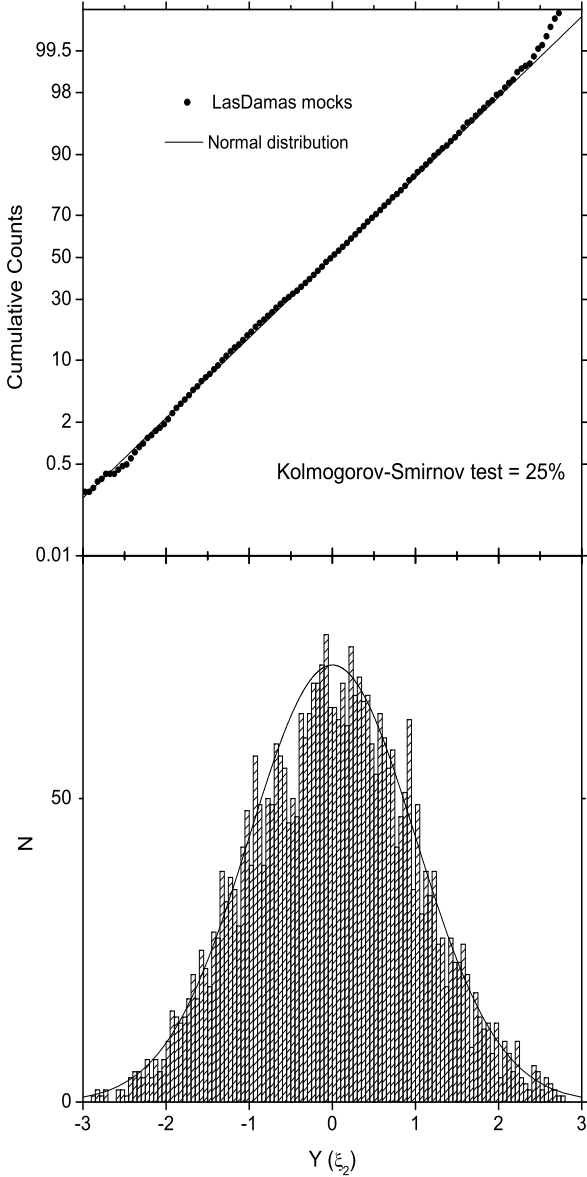


Figure 14. Histogram of the normalised scattering of ξ_2 measurements and their cumulative distribution from 80 mock LasDamas catalogs compared to the normal distribution with mean zero and unit variance.

4.3 Covariance matrix as a function of cosmological parameters

Another systematic effect in estimating covariance matrix is the dependence of \mathbf{C}^{stat} on the cosmological model. Our estimates of the covariance matrix are based on the mock catalogs that were created for a specific cosmological model, namely a spatially-flat Λ CDM with $\Omega_m = 0.25$, $\sigma_8 = 0.8$ assuming that the gravity is described well by GR. In other cosmological models or different values of parameters the intrinsic scattering in the correlation function and therefore the covariance matrix will be different. The scaling of \mathbf{C}^{stat} with cosmological parameters is extremely difficult to model theoretically for nontrivial survey volumes.

To estimate this effect we will again use the Fisher ma-

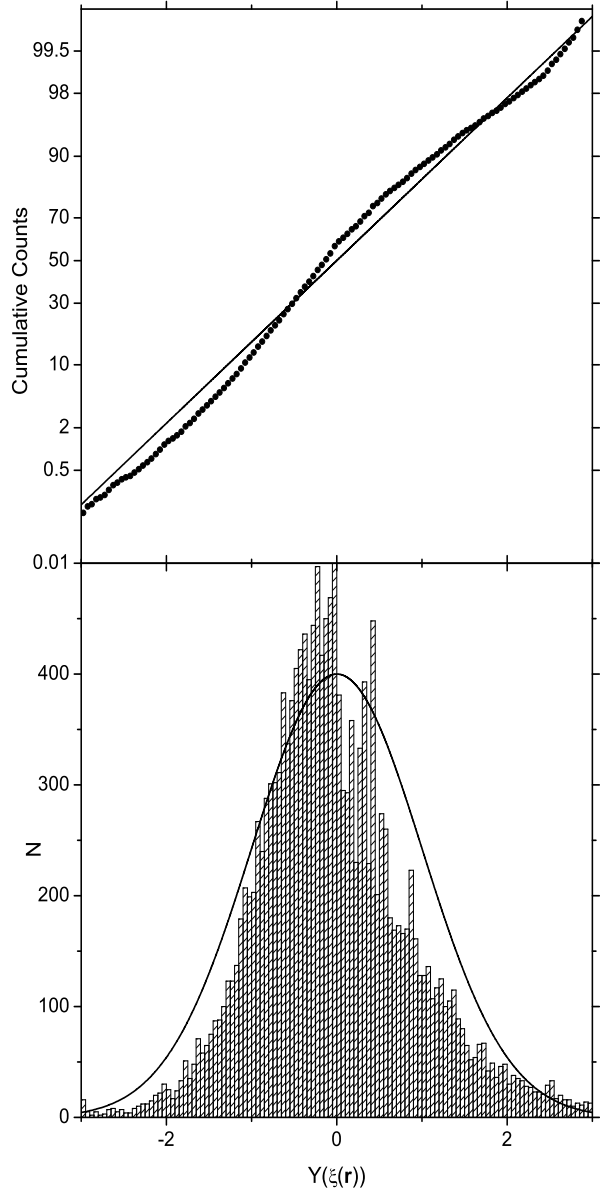


Figure 15. Histogram of the normalised scattering of $\xi(\sigma, \pi)$ measurements from 80 mock LasDamas catalogs.

trix calculations for an SDSS-II like survey. We compute a Fisher matrix $F(b, f, \alpha||, \alpha_{\perp}, \mathbf{p})$ for different values of cosmological parameters and look at how the expected errors on the measurements of growth scale. The uncertainties in the measurements of the power-spectrum can be schematically divided into two parts: coming from the cosmic variance and from the shot-noise. The shot-noise contribution depends on the total number of galaxies and their distribution in the survey volume and is insensitive to the underlying cosmological model. The cosmic variance component depends on the parameters determining the overall amplitude of the power-spectrum b , f and σ_8 , but is not very sensitive to the cosmological parameters describing its shape \mathbf{p} .

We derive Fisher matrix errors on the measurements of the growth parameter $f\sigma_8$ and bias $b\sigma_8$ for different fiducial values. This predictions are shown on Figs. 16 and 17.

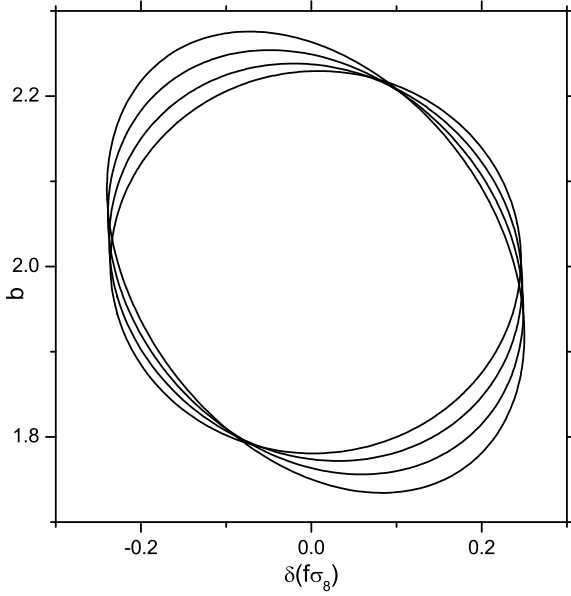


Figure 16. Fisher matrix predictions of the correlated errors of parameters b and $f\sigma_8$ from an SDSS-II like survey. Different contours correspond to the 1σ confidence level ellipses for the fiducial cosmologies with $f\sigma_8$ equal to 0.2, 0.3, 0.4 and 0.5 from largest to smallest ellipse respectively. Bias is fixed to $b = 2$. Horizontal line shows the deviation from fiducial value.

Figure 16 shows the size of 1σ ellipses for different fiducial values of $f\sigma_8$ when $b = 2$, while Fig. 17 shows the same ellipses for different values of $b\sigma_8$ when $f = 0.45$. The relative change is small compared to the sizes of the contours themselves. We conclude that this effect is relatively unimportant for the range of values $f\sigma_8$ and $b\sigma_8$ allowed by our data and ignore it in our analysis.

For next generation of surveys, however, the errors on the measurements of growth will be significantly smaller and this effect will have to be taken into account. This implies that deviations from the best-fit value towards stronger clustering amplitude will be more likely than deviations of the same magnitude towards weaker clustering amplitude.

4.4 Λ CDM and General Relativity

In a specific cosmological model the growth rate will depend on the parameters describing background geometry as well as the theory of gravity. Assumptions about exact nature of this dependence bring in a very strong theoretical priors that might affect the results of data analysis strongly. In our work we will always make three separate assumptions about how the growth rate depends on the background expansion from most restricting to almost premise free.

First we will assume that General Relativity (GR) is the correct theory of gravity. In this case the growth function $f^{\text{gr}}(z) = f(\mathbf{p}, z)$ can be computed at every redshift from basic cosmological parameters \mathbf{p} . The other two numbers that are necessary to completely describe the amplitude of the correlation function are the linear bias $b(z)$ and the overall amplitude of clustering $\sigma_8(z = 0)$. In this Λ CDM + GR model our cosmological parameters of interest will be $\mathbf{p} = (\Omega_m, h, w)$ and $\mathbf{A} = (b_i(z), \sigma_8)$.

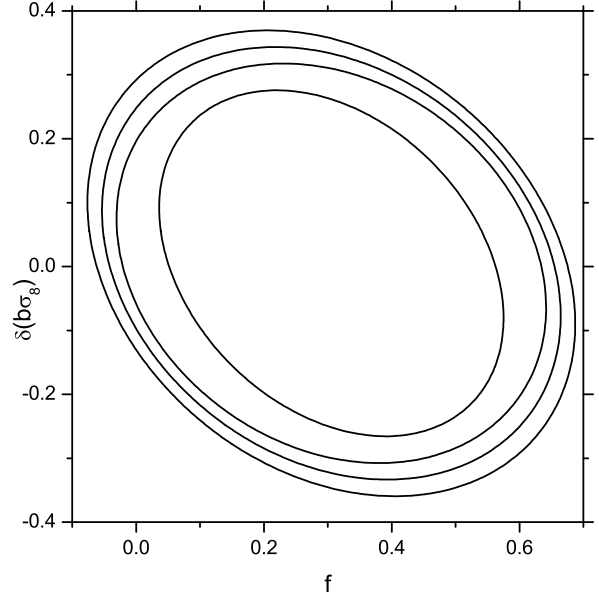


Figure 17. Fisher matrix predictions of the correlated errors of parameters $b\sigma_8$ and f from an SDSS-II like survey. Different contours correspond to the 1σ confidence level ellipses for the fiducial cosmologies with $b\sigma_8$ equal to 1.4, 1.5, 1.6 and 1.8 from outside to inside respectively. Growth rate is fixed to $f = 0.45$. Vertical line shows the deviation from fiducial value.

We will use the prior likelihood on \mathbf{p} and σ_8 from the WMAP7 measurements and SNIa data. We do this by using the relaxed MonteCarlo Markov Chain of this joint data.⁴ For every $b(z_i)$ we will go through the MCMC chain and for each value of \mathbf{p} and σ_8 compute the growth function $f(z)$ and then the theoretical correlation function. Afterwards we will marginalize over \mathbf{p} and σ_8 . This is equivalent to taking the following analytical integral

$$\mathcal{L}^{\text{gr}}(b(z_i)) = \int \mathcal{L}_{\text{tot}}(\mathbf{p}, \mathbf{A}) \mathcal{L}_{\text{prior}}(\mathbf{p}, \sigma_8) d\mathbf{p} d\sigma_8, \quad (30)$$

where $\mathcal{L}_{\text{prior}}$ is effectively given by the MCMC. This will enable us to derive constraints on the linear bias parameter $b(z)$ in two redshift bins.

4.5 γ parametrization of growth

For our second model we will consider the γ parametrization of growth (Linder 2005). In this model the growth function is assumed to depend on parameters \mathbf{p} as

$$f(z) = \left(\frac{\Omega_m(1+z)^3}{\Omega_m(1+z)^3 + (1-\Omega_m)(1+z)^{-3(1+w)}} \right)^\gamma, \quad (31)$$

where γ is a redshift and scale independent number. For $\gamma = 0.55$, Eq. (31) gives numerical results that are very close to the predictions of GR. If γ is larger than 0.55 the growth is weaker compared to GR and vice versa.

In this model $\mathbf{A} = (b(z_i), \gamma, \sigma_8)$. We will assume that the shape of the correlation function can still be accurately modelled by Λ CDM predictions and will use WMAP + SNIa MCMC to marginalize over \mathbf{p} and σ_8 as in Sec. 4.4.

⁴ Available for download from <http://lambda.gsfc.nasa.gov>.

To use the WMAP prior on σ_8 for γ parametrization we have to take into the account the fact that σ_8 is not directly measured by CMB experiments. The measured quantity is σ_8 at the last scattering surface with $z \approx 1100$ and then the $\sigma_8(z=0)$ is inferred by rescaling

$$\sigma_8(z=0) = \sigma_8(z=1100) \frac{G(z=0)}{G(z=1100)}, \quad (32)$$

where $G(z)$ is the growth factor assuming GR.

To make the priors on σ_8 as given by WMAP MCMC chain consistent with our assumption that the growth of structure is modified as in Eq. (31) we rescale the values of σ_8 in WMAP MCMC chain by

$$\sigma_8(z=0)^\gamma = \sigma_8(z=0)^{\text{GR}} \frac{G(z=1100)^{\text{GR}}}{G(z=1100)^\gamma} \frac{G(z=0)^\gamma}{G(z=0)^{\text{GR}}}, \quad (33)$$

where G^γ and G^{GR} are the growth functions computed in γ parametrization and GR respectively. After marginalization we will get a posterior likelihood function $\mathcal{L}^\gamma(b(z_i), \gamma)$. The measurements of γ in general will be correlated with the measurements of bias.

4.6 Free growth

In the last model we will not make any assumptions about the relationship between f and \mathbf{p} and will treat $f(z_i)$ in each redshift bin as a free parameter. In this model three parameters describing the amplitude f , b and σ_8 are degenerate and only two combinations of them can be measured independently. We will choose these combinations to be $b(z_i)\sigma_8(z_i)$ and $f(z_i)\sigma_8(z_i)$.

We will assume again that only the growth of the perturbations is different from the GR case and the overall shape of the correlation function can still be model by Λ CDM model. If we make this assumption we can use the same MCMC to marginalize over \mathbf{p} so that we are left with the posterior likelihood function $\mathcal{L}^{\text{fg}}(b(z_i)\sigma_8(z_i), f(z_i)\sigma_8(z_i))$.

5 RESULTS AND DISCUSSION

We use the method outlined in Sec. 4 to constrain parameters describing the redshift evolution of the clustering of LRGs. We first use only scales up to $60 h^{-1}$ Mpc and then use all scales up to $200 h^{-1}$ Mpc. Our results are presented in Tab. 1.

For the Λ CDM + GR model the small scale data constrains the real-space amplitude of the galaxy clustering signal in both redshift bins with the accuracy of about 5 percent. These measurements are consistent with previous estimates, showing that LRGs are highly biased tracers of the underlying matter field. The power spectrum amplitudes in the two redshift bins are close and consistent with the assumption of the constant clustering amplitude. The constraints improve slightly when we extend the analysis to include data on scales $60 - 200 h^{-1}$ Mpc. This inclusion results in slightly higher estimates of bias in both redshift bins, but the two measurements are consistent at a 1σ confidence level.

For the more general γ parametrization that has GR as a specific case, the γ parameter is constrained with the precision of about 16 percent. Including larger scale data does not improve the measurement error. Both large and small scale measurements prefer a weaker growth than in GR but are consistent with GR results at one σ confidence level. When the large scale data is included the best-fit values for γ are closer to the GR values. The γ parametrization fits give best-fit values of bias in both redshift bins that are slightly lower than the ones measured when assuming GR, following the standard degeneracy between the bias and the RSD signal.

Note that when adopting the γ parametrization, we have implicitly assumed that the growth is modified with respect to GR in a manner that is independent of the scale. Even if the real modifications of gravity are scale dependent, the γ parametrization will still be able to capture deviations from GR, but the measured γ will be an average over the scales being considered.

For the most general model of free growth the parameter $f\sigma_8$ can be measured with the accuracy of about 10 percent in both redshift bins. The inclusion of large scale data, again improves these constraints only slightly. This shows that at larger scales SDSS DR7 clustering data is noisier and introduces more scatter. The best fit values of growth, when it is allowed to freely vary are consistent with the predictions of GR. The large scale measurements are closer to the actual GR values than the measurements derived from the small scales only. In this model lower values of bias are required to fit data compared to the previous two.

The measurements of the pair of variables $b\sigma_8$, $f\sigma_8$ and $b\sigma_8$, γ are very weakly correlated and can be assumed to be independent for all practical purposes.

6 CONCLUSIONS

In this paper we have considered systematic deviations from the linear plane-parallel RSD model for the large scale clustering of galaxies. These include systematic deviations due to wide-angle and non-linear effects, and problems caused by inaccurate modelling of the redshift distribution. By testing different models against the measurements from N-body simulations we checked that, by including these effects, we can fit simulated large-scale RSD data extremely well. We have also considered the relative importance of these effects, showing that the wide-angle effects are small for the SDSS DR7 survey and can be safely ignored even on scales as large as $200 h^{-1}$ Mpc, but nonlinear damping of the Baryon Acoustic Oscillation (BAO) peak (Meikson et al. 1999) and the non-isotropic μ distribution effects have to be taken into account in order to properly fit the data.

Different ways of extracting RSD information have been considered before, including a fit to the two-dimensional correlation function $\xi(\sigma, \pi)$ and the normalised quadrupole Q . We argue that the best approach is to perform a joint fit to measured Legendre momenta of the correlation function. Based on the simple linear plane-parallel model they contain exactly the same information as $\xi(\sigma, \pi)$ and their measurement errors are more Gaussian, which makes the interpretation of ξ_ℓ straightforward. Compared to only using the normalised quadrupole Q , they contain significantly more infor-

Model	Variable	Scales less than 60 Mpc/h	Scales up to 200 Mpc/h	“Standard” model expectation
wCDM	$b(z_1)\sigma_8(z_1)$	1.4949 ± 0.0772	1.5175 ± 0.0760	
	$b(z_2)\sigma_8(z_2)$	1.5316 ± 0.0717	1.57435 ± 0.0672	
γ	$b(z_1)\sigma_8(z_1)$	1.5462 ± 0.0911	1.4402 ± 0.0558	
	$b(z_2)\sigma_8(z_2)$	1.5522 ± 0.0916	1.5063 ± 0.0433	
	γ	0.6545 ± 0.1100	0.5916 ± 0.1165	0.55
Free growth	$b(z_1)\sigma_8(z_1)$	1.4736 ± 0.0634	1.4366 ± 0.0575	
	$b(z_2)\sigma_8(z_2)$	1.4553 ± 0.0498	1.5021 ± 0.0425	
	$f(z_1)\sigma_8(z_1)$	0.3929 ± 0.0453	0.3410 ± 0.0508	0.4260
	$f(z_2)\sigma_8(z_2)$	0.4326 ± 0.0357	0.4509 ± 0.0417	0.4367

Table 1. Constraints on parameters describing growth and clustering bias of galaxies with respect to the matter field in different models with and without including measurements from scales more than $60 h^{-1}$ Mpc. “Standard” model refers to the spatially-flat Λ CDM with $\Omega_m, \sigma_8 = 0.8$ and general relativity.

mation and allow for the measurements of bias and growth independently instead of measuring only their ratio. Also Q was originally proposed because it was believed to have certain advantages of being independent of the shape of the power-spectrum and nonlinear effects. We show that that does not hold on large scales: Q is affected by nonlinearities as much as the correlation itself and it is still affected by AP effect and the dependence on the shape of the power-spectrum and on the background cosmological parameters is not completely removed.

We have analysed the SDSS DR7 LRG clustering in redshift-space and obtained constraints on bias and parameters describing structure growth in two redshift bins. We have presented what we consider to be a very robust analysis, taking into account all of the effects that could influence the redshift-space correlations function. The inclusion of the very large scale data does not improve our measurements of bias and growth parameters significantly: current measurements of the correlation function on the scales larger than $60 h^{-1}$ Mpc are too noisy to be of practical interest. The next generation of ongoing and planned surveys such as *BOSS*; Schlegel et al. 2009), *BigBOSS* and the ESA *Euclid* mission (Laureijs et al. 2009) will enable us to measure clustering properties of galaxies on very large scales with high accuracy. For these surveys where the measurements are more precise, the full treatment of RSD effects will be very important. In addition, there will be significantly more information available on the largest scales.

ACKNOWLEDGEMENTS

LS is grateful for support from the European Research Council. WJP is grateful for support from the UK Science and Technology Facilities Council, the Leverhulme trust and the European Research Council. AR is grateful for the support from a UK Science and Technology Facilities Research Council (STFC) PhD studentship. We thank Beth Reid for useful comments on an early draft of this paper and Marc Manera for useful discussions. LS acknowledges partial support from Georgian National Science Foundation grant GNSF ST08/4-442 and SNFS SCOPES grant no. 128040.

REFERENCES

- Abazajian, K. N., et al., 2009, *ApJS*, 182, 543
Alcock C., Paczynski B., 1979, *Nature*, 281, 358
Ballinger W. E., Peacock J. A., Heavens A. F., 1996, *MNRAS*, 282, 877
Barrow J. D., Bhasvar S. P., Sonoda D. H., 1984, *MNRAS*, 210, 19
Bharadwaj S., 1996, *ApJ*, 472, 1
Cabr   A., Fosalba P., Gazta  aga E., Manera M., 2008, 381, 1347
Cabr   A., Gazta  aga E., 2009, *MNRAS*, 393, 1183
Carlson J., White M., Padmanabhan N., 2009, *PRD*, 80, 043531
Cole S., Fisher K.B., Weinberg D.H., 1995, *MNRAS*, 275, 515
Crocce M., Scoccimarro R., 2006, *PRD*73, 063519
Colless M., et al., 2003, preprint [astro-ph/0306581]
Crocce M., Scoccimarro R., 2008, *PRD*77, 023533
Dalal N., Dor   O., Huterer D., Shirokov A., 2008, *PRD*, 77, 123514
Desjaques V., Seljak U., 2010, preprint, (arXiv:1006.4763 [astro-ph.CO])
Desjaques V., Sheth R. K., 2010, *Phys. Rev. D*, 81, 023526
Eisenstein D.J., et al., 2001, *AJ*, 122, 2267
Eisenstein D. J., Seo H.-J., White M., 2007, *ApJ*, 665, 14
Feldman H.A., Kaiser N., Peacock J.A., 1994, *MNRAS*, 269, 426
Feldman H. A., Watkins R., Hudson M. J., 2010, *MNRAS*, 407, 2328
Fisher K.B., 1995, *ApJ*, 448, 494
Fukugita, M., Ichikawa, T., Gunn, J. E., Doi, M., Shimasaku, K., Schneider, D. P., 1996, *AJ*, 111, 1748
Gunn, J. E., et al., 1998, *AJ*, 116, 3040
Guzzo L. et al., 2009, *Nat.*, 461, 451
Hamilton A.J.S., 1992, *ApJ*, 385, L5
Hamilton A.J.S., 1997, preprint (arXiv:astro-ph/9708102)
Hawkins E., et al., 2003, *MNRAS*, 346, 78
Jackson J.C., 1972, *MNRAS*, 156, 1
Jennings E., Baugh C. M., Pascoli C., 2011, 727, L9
Jing Y.P., B  rner G., 2004, *ApJ*, 617, 782
Kaiser N., 1987, *MNRAS*, 227, 1
Kashlinsky A., Atrio-Barandela F., Kocevski D., Ebeling H., 2009, *ApJ*, 686, L49
Kazin E., et al., 2010, *ApJ*, 710, 1444

- Landy, S. D., Szalay, A. S., 1993, *ApJ*, 412, 64
- Laureijs R. et al., 2009, *Euclid* Assessment Study Report for the ESA Cosmic Visions, (arXiv:0912.0914 [astro-ph.CO])
- Lewis A., Challinor A., Lasenby A., 2000, *ApJ*, 538, 473
- Li C., Jing Y.P., Kauffmann G., Börner G., Xi K., Wang L., 2007, *MNRAS*, 376, 984
- Linder E., 2005, *PRD*, 72, 043529
- Lucey J. R., 1979, PhD thesis
- Macaulay E., Feldman H., Ferreira P. G., Hudson M. J., Watkings R., 2011, preprint, (arXiv:1010.2651 [astro-ph.CO])
- Matsubara T., 2004, *ApJ*, 615, 573
- Matsubara T., 2008a, *PRD*, 77, 063530
- Matsubara T., 2008b, *PRD*, 78, 083519
- McBride C., et al., 2011, in prep
- Meikson A., White M., Peacock J. A., 1999, *MNRAS*, 304, 851
- Mo H. J., Jing Y. P., Börner G., 1992, *ApJ*, 392, 452
- Norberg P., Baugh C.M., Gaztañaga E., Croton D.J., 2009, *MNRAS*, 396, 19
- Nusser A., Davis M., 2010, preprint, (arXiv:1101.1650 [astro-ph])
- Okamura T., Jing Y. P., 2011, *ApJ*, 726, 11
- Padmanabhan N., et al., 2005, *PRD*, 72, 043525
- Papai P., Szapudi I., 2008, *MNRAS*, 389, 292
- Peacock J.A., Dodds S.J., 1996, *MNRAS*, 280, L19
- Percival W. J. et al., 2004, *MNRAS*, 385, L78
- Percival W. J. et al., 2010, *MNRAS*, 401, 2148
- Press W.H., Teukolsky S.A., Vetterling W.T., Flannery B.P., 1992, *Numerical recipes in C. The art of scientific computing*, Second edition, Cambridge: University Press.
- Raccanelli A., Samushia L., Percival W. J., 2010, *MNRAS*, 409, 1525
- Reid B. A., et al., 2010, *MNRAS*, 404, 60
- Samushia L., et al. 2010, *MNRAS*, in press
- Schlegel D., White M., Eisenstein D.J., 2009, preprint (arXiv:0902.4680 [astro-ph.CO])
- Schlegel et al., 2009, preprint (arXiv:0904.0468 [astro-ph.CO])
- Scoccimarro R., 2001, *Ann. New York Acad. Sci.*, 927, 13
- Scoccimarro R., 2004, *PRD*, 083007
- Seljak U., Hamaus N., Desjacques V., 2009, *PRL* 103, 091303
- Simpson F., Peacock J., 2010, *PRD*, 81, 043512
- Smith R. E., Peacock J. A., Jenkins A., White S. D. M., et al., 2003, *MNRAS*, 341, 1311
- Song Y.-S., Sabiu C., Nichol B., Kayo I., 2010, preprint (arXiv:1006.4630 [astro-ph.CO])
- Szalay A. S., Matsubara T., Landay S. D., 1998, *ApJ*, 498, L1
- Szapudi I., *PRD*, 70, 083536
- Takada M., *PRD*, 2006, 74, 043505
- Taruya A., Nishimichi T., Saito S., 2010, *PRD*, 063522
- Tegmark M. et al., 2006, *PRD*, 74, 123507
- Thomas S. A., Abdalla F. B., Lahav O., 2010, preprint (arXiv:1012.2272 [astro-ph.CO])
- Tocchini-Valentini D., Barnard M., Bennett C. L., Szalay A. S., 2011, preprint (arXiv:1101.2608 [astro-ph.CO])
- Watkins R., Feldman H. A., Hudson M. J., 2009, *MNRAS*, 392, 743
- York D.G., et al., 2000, *AJ*, 120, 1579
- Zaroubi S., Hoffman Y., 1993, preprint (arXiv:astro-ph/9311013)
- Zehavi I. et al., 2005, *ApJ*, 621, 22